Multi-Period Optimal Energy Flow in Integrated Electricity and Gas Systems With Alternative Gas Injection Considering Gas Composition Dynamics

Sheng Wang, *Member, IEEE,* Hongxun Hui, *Member, IEEE,* Tao Chen, *Member, IEEE*

***Abstract*—Injecting alternative gas (e.g., green hydrogen from renewable generations) into the natural gas system is a promising way to decarbonize the energy system. However, the alternative gas injection could be time-varying due to the stochastic renewable generations. It could lead to fluctuations in the gas compositions across the gas network, adversely affecting the secure operation of integrated electricity and gas systems (IEGS). For managing the operating condition and guaranteeing the security of IEGS during operation, this paper proposes a multi-period optimal energy flow model (MPOEF) for IEGS with alternative gas injections. First, a convex hull of the gas security range is derived from the Dutton method. Then, the MPOEF is proposed to mitigate the impacts of alternative gas injection on gas security over the entire operational period. Both the dynamics of gas composition and gas flow are modeled, which can accurately describe the travel of alternative gas concentrations at the real-time level. The dynamics in the gas mixture properties (e.g., specific gravity) are modeled as variables to fully reveal the impacts of time-varying gas compositions. To tackle the high non-convexities in the MPOEF problem, second-order-cone relaxation is well-tailored and firstly used in the case of varying gas compositions, making the motion equations and advective transport equations more tractable. An advanced second-order-cone sequential programming is devised to drive the relaxation tight more efficiently. Finally, an illustrative case is used to validate the proposed method.**

***Index Terms*—alternative gas, gas composition, hydrogen, integrated electricity and gas systems, optimal energy flow, power to gas**

I. Introduction

ALTERNATIVE gas (e.g., green hydrogen, methane, etc.) is one of the most appealing solutions to low-carbon energy systems. It is usually produced through power-to-gas (PTG) facilities by consuming surplus renewable generations. It can be blended with the existing natural gas in the pipeline, and then transported to various locations to satisfy the gas demand [1]. Many countries have started their early trials for alternative gas blending projects. For example, the UK launched its first phase hydrogen blending project "HyDeploy" in 2017, which provided gas to over 100 homes and 30 university buildings at Keele University [2]. In 2019, China launched its first commercial demonstration project on hydrogen blending in Chaoyang, which safely runs for one year with 10% hydrogen concentration [3]. Because PTGs highly rely on electricity supply, the electricity and gas system are ever-increasingly interdependent and are therefore regarded as an integrated electricity and gas systems (IEGS).

Due to the stochastic nature of renewable generations, alternative gas injection also fluctuates. It could lead to variations of gas compositions across the gas network, endangering the normal operation of the IEGS. For example, hydrogen has a lower gross caloric value (GCV) than natural gas. With the increase of the hydrogen content, the GCV of the new gas mixture will decrease. Gas is usually used for combustion to produce heat energy, and the gas appliances are also usually tested under a specified gas composition. The uncertain gas composition will cause unsatisfactory combustion, and could further shorten the lifespans of the gas appliances [4]. Moreover, the fraction of hydrogen also affects the physical properties of the gas mixture (e.g., specific gravity), leading to variations in gas flow and nodal pressure patterns across the gas network. It could also cause linepack swings, adversely affecting the system components (e.g., pipelines, valves) [5]. Therefore, under uncertain and distributed injections of hydrogen from renewable energies, the gas composition needs to be regulated within the secured range from the perspective of the safe operation of the whole IEGS.

So far, most studies focus on the simulation of the gas composition across the gas network with alternative gas injections. For example, the simulation technique of the gas composition in the gas network is proposed in [6] based on the steady-state model. The mathematical model of natural gas and alternative gas mixtures in the transmission pipeline networks under steady-state conditions is studied in [7] using a non-isothermal approach. The IEGS is modeled to address the increasingly distributed photovoltaic generations and their hydrogen production in [8]. The gas distribution network is also used to absorb the excess renewable electricity generation through hydrogen injections in [9], where a steady-state analysis is carried out to identify the critical nodes with potential Wobbe index violations. The probabilistic natural gas and hydrogen flow model is established in [10] considering multiple uncertainties. The impacts of different hydrogen blending modes on the IEGS are investigated in [11]. However, these simulation-orientated studies only focus on the impact analysis of hydrogen injections, which is rather passive. In other words, if the system security is violated, these studies cannot provide quantitative suggestions or active measures to recover gas system security by regulating the operating condition of IEGS components.

Recently, several studies begin to investigate the optimal operation strategies of the IEGS with varying gas compositions. Compared with the simulation-orientated studies, these optimization-orientated studies with active decision-making can help the system operator to improve the cost-benefits and securities under alternative gas injections. A coordinated optimal operation framework of IEGS considering gas composition tracking is developed in [12]. The aggregated flexibility from multiple PTG units considering the gas composition control is explored in [13]. A distributionally robust hydrogen

optimization with ensured security and multi-energy couplings is proposed in [14]. The volt-VAR-pressure optimization is studied in the distribution-level IEGS in the presence of hydrogen injections in [15]. An optimal energy flow model of IEGS with alternative gas is studied in [16] to maintain gas security.

A common drawback of the aforementioned studies is that their optimization models are formulated on a steady-state basis, where the dynamics in the gas system are usually ignored. Due to the intermittency of the renewable generations, the hydrogen injections, gas compositions, etc., in the gas network, are highly fluctuated during the operation process. Since the gas dynamics are far slower than the electricity system, it will be inaccurate to ignore the gas dynamics if the optimization model is applied to the operational horizon. There are two types of dynamics in gas systems. The first is the gas flow dynamics, which have been widely modeled in the IEGS operation and scheduling problems in previous studies [17], [18]. The other one is the gas composition dynamics, which is unique in the gas system with varying gas compositions. It describes how a certain gas content travels across the gas network. For example, if hydrogen is injected at the beginning of a pipeline, it will be gradually transported to the end of the pipeline, so the gas composition at the end of the pipeline can remain unchanged for a short period.

Considering both gas flow and gas composition dynamics in the optimal operation of IEGS is both a necessary and challenging task, which has not been well addressed yet. The gas composition dynamics are governed by a set of nonlinear partial derivative equations (PDEs). Incorporating these terms will make the optimization model non-convex and time-interdependent, which not only increase the computation burden dramatically, but also make the problem intractable. Moreover, the travel of gas composition brings inconsistency to the physical properties (e.g., specific gravity, GCV, etc.) of the gas mixture in the gas network, which also brings high nonconvexities to the gas flow equations as well. Due to the above reasons, though the gas composition dynamics have been studied in traditional gas network simulations [19]–[21], it has seldom been incorporated in the coordinated optimal operation of IEGS [22]. There is merely a tractable and high-efficient solution method to this optimization problem with dynamic gas compositions yet.

To address the aforementioned research gaps, this paper develops the modeling and solution methods for the multi-period optimal energy flow (MPOEF) problem in IEGS with alternative gas injections considering the gas composition dynamics. The major contributions are summarized as follows:

(1) An MPOEF model of IEGS with alternative gas injections considering the gas composition dynamics is proposed. Compared with previous steady-state gas composition tracking models (e.g., [12], [14], etc.): 1) by modeling both the dynamics in gas flow and gas composition, our model can accurately characterize the travel of alternative gas concentrations across the gas network at the real-time level. 2) The dynamics in the physical properties of the gas mixtures (e.g., specific gravity, GCV, etc.) are modeled as variables, so that the impacts of alternative gases at the nodal scale can be comprehensively revealed and controlled. 3) The concept of linepack energy is developed for setting the terminal conditions, which can utilize the gas system flexibility to hedge against the fluctuating hydrogen injections during the operation, while still maintaining the robustness of the gas system at the end of the operation.

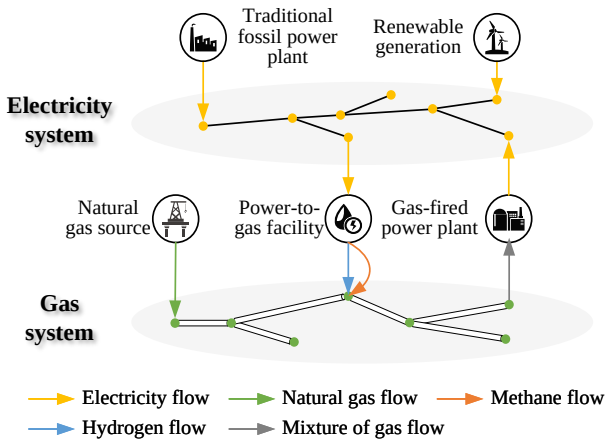

Fig. 1. Structure of the IEGS with alternative gas injections.

(2) A tractable solution method for the highly non-convex MPOEF problem is proposed. The second-order cone (SOC) reformulation is first tailored in this paper to convexify the discretized motion and advective transport PDEs in the presence of varying gas compositions. It can retain the 2nd-order information of these constraints to improve the computation efficiency. Advanced sequential SOC programming is applied with adaptive penalty factors, so that convergence and optimality can be well guaranteed.

(3) The convex hull of the gas security range that is defined by the Wobbe index (WI), incomplete combustion factor (ICF), soot index (SI), and flame speed factor (FS) is derived. Compared with the traditional Dutton method [23], it can 1) guarantee the convexity of the MPOEF problem by linearizing the security constraints; 2) better control the security of the IEGS in the presence of hydrogen by introducing the FS index.

II. Convex Hull of Gas Security Range

The structure of the IEGS with alternative gas injections is presented in Fig. 1. The IEGS contains two layers, namely, the electricity system and the gas system. The electricity system relies on traditional fossil power plants (TPP) (which uses fuels other than gas to generate electricity), renewable generators, and gas-fired power plants (GPP) to generate electricity. In the gas system, the gas supply mainly comes from natural gas sources. PTGs consume electricity to produce hydrogen and methane. They will be mixed in the gas network, and then transported to other locations to satisfy various gas demands.

Due to the different gas compositions of gas sources and PTGs, the gas compositions may vary across the gas network. As discussed in the introduction, gas appliances and system components have requirements for gas composition to operate safely. The gas security requirements vary by country and region. Here we use a typical Dutton method to constrain gas security, which is widely used in the UK, Australia, etc., as shown in the left half of Fig. 2 [24]. Different gas compositions

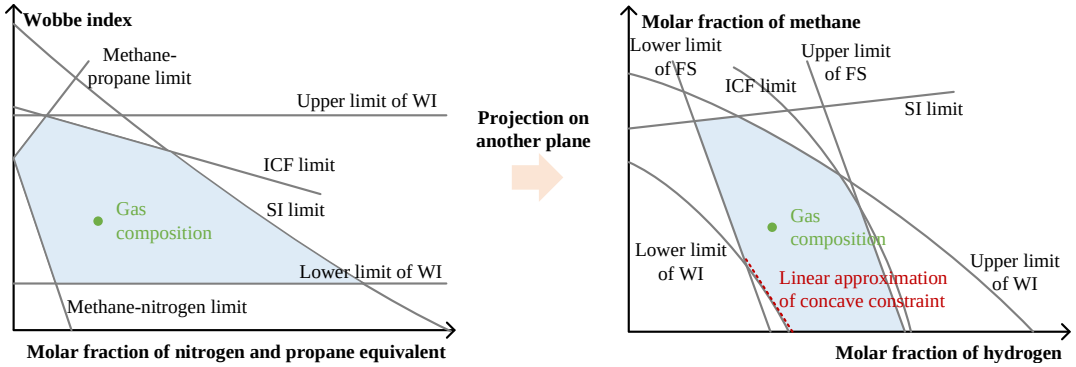

Fig. 2. Security ranges for gas composition using Dutton diagram.

have different coordinates in the Dutton diagram. The security range is outlined by a couple of security indices and physical constraints, including the WI, ICF, SI, etc [25]. To characterize the impacts of the higher flame speed of hydrogen, the Weaver flame speed factor (FS) is additionally introduced to the Dutton method in our study [26]. Though the Dutton diagram is convex in its own plane, when we need to track the gas compositions, it will become nonconvex when being projected on the plane that is formed by the molar fractions of different gas components, as shown in the right half of Fig. 2. It leads to a nonconvex security range, and will cause the MPOEF problem to be intractable. Therefore, we formulate the convex hull of the gas security range by linearizing the gas security functions:

$$\begin{aligned}\mathbb{H} = \Big\{ \boldsymbol{\chi}_{i,k} \mid\ & WI^{min} \le WI_{i,k} \le WI^{max};\\ & ICF_{i,k} \le ICF^{max}; SI_{i,k} \le SI^{max};\\ & FS_{i,k}^{min} \le FS_{i,k} \le FS_{i,k}^{max};\\ & 0 \le \chi_{i,k}^{hy} \le \chi^{hy,max}; \mathbf{0} \le \boldsymbol{\chi}_{i,k} \le \mathbf{1};\\ & \mathbf{1}^T \boldsymbol{\chi}_{i,k} = 1; \Big\}, \forall i \in \mathcal{I}, \forall k \in \mathcal{K} \end{aligned} \tag{1}$$

$$WI_{i,k} = GCV_{i,k} / \left((S^{ng})^{\frac{1}{2}} + (S^{ng})^{-\frac{1}{2}} S_{i,k} \right) \tag{2}$$

$$ICF_{i,k} = (WI_{i,k} - 50.73 + 0.03\chi_{i,k}^{np})/1.56 - 0.01\chi_{i,k}^{hy} \tag{3}$$

$$\begin{aligned} SI_i = 0.896 tan^{-1}(& 0.0255\chi_{i,k}^{pr} - 0.0233\chi_{i,k}^{ni}\\ & -0.0091\chi_{i,k}^{hy} + 0.617) \end{aligned}$$

$$FS_{i,k} = \frac{\sum_{n \in \mathcal{N}} \chi_{i,k,n} f s_n}{AF + 5\chi_{i,k}^{ni} - 18.8\chi_{i,k}^{ox} + 1} \tag{4}$$

where $\mathbb{H}$ is the gas security range in the normal condition; $\boldsymbol{\chi}_{i,k}$ is the set of gas compositions at bus i at time step k; $\chi_{i,k}^{np}$ is the total molar fraction of propane and nitrogen; $\chi_{i,k}^{hy}$, $\chi_{i,k}^{pr}$, $\chi_{i,k}^{ni}$, and $\chi_{i,k}^{ox}$ are the molar fractions of hydrogen, propane, nitrogen, and oxygen, respectively; $WI_{i,k}$, $ICF_{i,k}$, $SI_{i,k}$, $FS_{i,k}$, $GCV_{i,k}$, and $S_{i,k}$ are the WI, ICF, SI, FS, GCV, and specific gravity of the gas mixture at bus i in time step k, respectively; S^{ng} is the specific gravity of natural gas; WI^{min} and WI^{max} are the lower and upper bounds of WI, respectively; ICF^{max}, SI^{max}, and $\chi^{hy,max}$ are the upper bounds of ICF, SI, and molar fraction of hydrogen, respectively; $\mathcal{I}$ and $\mathcal{K}$ are the sets of buses and time steps, respectively; fs_n is the burning velocity of gas component n in a stoichiometric air mixture; AF is the air-fuel ratio.

The nodal GCV and specific gravity are related to the nodal gas composition, which can be calculated as:

$$GCV_{i,k} = \sum_{n \in \mathcal{N}} GCV_n \chi_{i,k,n} \tag{5}$$

$$S_{i,k} = \sum_{n \in \mathcal{N}} M_n \chi_{i,k,n} / M^{air} \tag{6}$$

where $\mathcal{N}$ is the set of gas components; GCV_n and M_n are the GCV and molecular weight of gas component n, respectively; $\chi_{i,k,n}$ is the molar fraction of gas component n at bus i in time step k; M^{air} is the molecular weight of air.

III. MPOEF Model

When the renewable generation fluctuates, the alternative gas injection will also be fluctuated, which may cause the gas compositions in the gas network to violate the secure range. The MPOEF model is developed to accommodate the alternative gas injection in a secure way. The objective of the MPOEF is to minimize the total cost of electricity generation and gas production over the operational horizon, by regulating the real-time operating conditions of IEGS components (e.g., gas sources, PTGs, GPPs, TPPs, renewable generations, etc.), as shown below:

$$C^T = \sum_{k \in \mathcal{K}} \left(\sum_{i \in \mathcal{I}} \sum_{l \in \mathcal{L}_i^{tpp}} cst_{i,l}(g_{i,l,k}^{tpp}) + \sum_{i \in \mathcal{I}} \sum_{l \in \mathcal{L}^s} \mu_{i,l}^s q_{i,l,k}^s \right) \tag{7}$$

where C^T is the total cost; $\mathcal{I}$ is the set of gas buses; $\mathcal{L}_i^{tpp}$ and $\mathcal{L}_i^s$ are the sets of TPPs and gas sources at bus i, respectively; $g_{i,l,k}^{tpp}$ is the electricity generation of TPP l at bus i in time step k; $q_{i,l,k}^s$ is the gas production of gas source l at bus i at time step k; $cst_{i,l}$ is the cost function of TPP l at bus i; $\mu_{i,l}^s$ is the nodal price for the gas production of gas source l at bus i.

In the following subsections, the constraints of the MPOEF problem will be modeled in detail.

A. Model of Gas System

1) Model of the gas system dynamics: In a horizontal and isothermal pipeline, the gas mixture flow is governed by the

following three sets of PDEs, namely, continuity equation, motion equation, and advective transport equation [27], [28]:

$$\frac{A_{ij}}{\rho_0}\frac{\partial \rho_{ij}}{\partial t}+\frac{\partial q_{ij}}{\partial x}=0 \tag{8}$$

$$\frac{\partial p_{ij}}{\partial x}+\frac{\rho_0}{A_{ij}}\frac{\partial q_{ij}}{\partial t}+\Theta_{ij}^2\frac{1}{\rho_{ij}}q_{ij}|q_{ij}|=0 \tag{9}$$

$$\frac{\partial \chi_{ij,n}}{\partial t}+\frac{\rho_0}{A_{ij}}\frac{q_{ij}}{\rho_{ij}}\frac{\partial \chi_{ij,n}}{\partial x}=0,\ n\in\mathcal{N} \tag{10}$$

where p_{ij}, q_{ij}, and ρ_{ij} are the pressure, flow rate, and density of the gas in pipeline ij, respectively; $\chi_{ij,n}$ is the gas composition of component n. These four variables are all functions of time t and distance x; A_{ij} is the cross-section area of the pipeline that connects bus i and j (which is denoted as pipeline ij for conciseness); ρ_0 is the gas density in the standard temperature and pressure condition; $\Theta_{ij}^2=\frac{8f_{ij}\rho_0^2}{\pi^2 D_{ij}^5}$, where f_{ij} and D_{ij} are the friction factor and diameter of pipeline ij, respectively [29].

Let: $\overline{\rho}_{ij,m,k}=(\rho_{ij,m,k+1}+\rho_{ij,m+1,k+1})/2$, $\Delta\rho^t_{ij,m,k}=(\rho_{ij,m,k+1}-\rho_{ij,m,k}+\rho_{ij,m+1,k+1}-\rho_{ij,m+1,k})/2$, $\Delta q^x_{ij,m,k}=q_{ij,m+1,k+1}-q_{ij,m,k+1}$, $\Delta q^t_{ij,m,k}=(q_{ij,m+1,k+1}-q_{ij,m+1,k}+q_{ij,m,k+1}-q_{ij,m,k})/2$, $\overline{q}_{ij,m,k}=(q_{ij,m,k}+q_{ij,m+1,k}+q_{ij,m,k+1}+q_{ij,m+1,k+1})/4$, $\Delta p^x_{ij,m,k}=p_{ij,m+1,k+1}-p_{ij,m,k+1}$, $\Delta\chi^t_{ij,m,k,n}=(\chi_{ij,m,k+1,n}-\chi_{ij,m,k,n}+\chi_{ij,m+1,k+1,n}-\chi_{ij,m+1,k,n})/2$, and $\Delta\chi^x_{ij,m,k,n}=\chi_{ij,m+1,k+1,n}-\chi_{ij,m,k+1,n}$, where $\rho_{ij,m,k}$, $q_{ij,m,k}$, and $p_{ij,m,k}$ are the density, gas flow, and gas pressure at segment m in pipeline ij at time step k; $\chi_{ij,m,k,n}$ is the gas composition of gas component n segment m in pipeline ij at time step k.

Then, we can discretize the above PDEs into:

$$\frac{A_{ij}}{\rho_0}\frac{\Delta\rho^t_{ij,m,k}}{\Delta t}+\frac{\Delta q^x_{ij,m,k}}{\Delta x}=0 \tag{11}$$

$$\frac{\Delta p^x_{ij,m,k}}{\Delta x}+\frac{\rho_0}{A_{ij}}\frac{\Delta q^t_{ij,m,k}}{\Delta t}+\gamma_{ij}\Theta^2\frac{\overline{q}^2_{ij,m,k}}{\overline{\rho}_{ij,m,k}}=0 \tag{12}$$

$$\frac{\Delta\chi^t_{ij,m,k,n}}{\Delta t}+\frac{\rho_0}{A_{ij}}\frac{\overline{q}_{ij,m,k}}{\overline{\rho}_{ij,m,k}}\frac{\Delta\chi^x_{ij,m,k,n}}{\Delta x}=0,\quad ij\in\mathcal{GP},m\in\mathcal{M},k\in\mathcal{K},n\in\mathcal{N} \tag{13}$$

where $\mathcal{M}$ is the set of pipeline segments, respectively; Δt and Δx are the time step and length step, respectively; $\gamma_{ij}=sgn(q_{ij}|_{t=0})$ represents the direction of gas flow at $t=0$ (we assume the gas flow does not change the direction during the operation); $sgn(\cdot)$ is the signum function.

According to the state equation of gas, the density and pressure of the gas should obey:

$$p_{ij,m,k}=z_{ij,m,k}r_{ij,m,k}T_0\rho_{ij,m,k} \tag{14}$$

where $z_{ij,m,k}$ and $r_{ij,m,k}$ are the compressibility factor and gas constant of the gas mixture at segment m in pipeline ij in time step k, respectively; T_0 is the temperature of the gas mixture, which we assume does not change during the operation.

It should be noted that different from the traditional gas flow model with constant gas composition, the gas constant here is a variable depending on the gas composition:

$$r_{ij,m,k}=\sum_{n\in\mathcal{N}}\chi_{ij,m,k,n}R_n \tag{15}$$

where R_n is the gas constant of gas component n.

2) Initial and boundary conditions: The above PDEs are formulated for each pipeline ij in the gas system. To solve the PDEs, initial and boundary conditions should be given. The initial condition is given as the operating state of the IEGS when $t=0$ (i.e., $p_{ij,m,1}=\hat{p}_{ij,m}$, $q_{ij,m,1}=\hat{q}_{ij,m}$, $\chi_{ij,m,1,n}=\hat{\chi}_{ij,m,n}$, where $\hat{p}_{ij,m}$, $\hat{q}_{ij,m}$, and $\hat{\chi}_{ij,m}$ can be obtained by solving the steady-state optimal energy flow problem with alternative gas at $t=0$ [16]).

The boundary conditions of the pipeline are determined by the pipelines and components that it connects with. As shown in (16) and (17), all the gas pressures at the connection points of the pipelines should be equal. Eq. (18) describes the nodal energy conservation for each gas component. Eqs. (19) and (20) describe that the gas compositions of pipelines at the connection point should be the same.

$$p_{ij,1,k}=p_{i,k}=p_{ij',1,k},\forall j'\in\mathcal{J}_i \tag{16}$$

$$p_{ij,M,k}=p_{j,k}=p_{i'j,M,k},\forall i'\in\mathcal{I}_j \tag{17}$$

$$\sum_{l\in\mathcal{L}_i^s}q^s_{i,l,k,n}-q^d_{i,k,n}+\sum_{l\in\mathcal{L}_i^{ptg}}q^{ptg}_{i,l,k,n}-\sum_{l\in\mathcal{L}_i^{gpp}}q^{gpp}_{i,l,k,n}-\sum_{j\in\mathcal{J}_i}q_{ij,1,k,n}=0,\forall n\in\mathcal{N} \tag{18}$$

$$(\gamma_{ij}+1)\chi_{ij,1,k,n}=(\gamma_{ij}+1)\chi_{i,k,n},\forall n\in\mathcal{N} \tag{19}$$

$$(\gamma_{ij}-1)\chi_{ij,M,k,n}=(\gamma_{ij}-1)\chi_{j,k,n},\forall n\in\mathcal{N} \tag{20}$$

where $p_{ij,1,k}$ and $p_{ij,M,k}$ represents the gas pressure at the 1st and M_{th} segments in pipeline ij in time step k, respectively; $p_{i,k}$ is the nodal gas pressure at bus i in time step k; $\mathcal{J}_i$ and $\mathcal{I}_j$ are the sets of buses connect with bus i and bus j, respectively; $q^d_{i,k,n}$ is the demand of gas component n at bus i; $\mathcal{L}_i^{gpp}$ and $\mathcal{L}_i^{ptg}$ are the set of GPPs and PTGs at bus i, respectively; $q^{gpp}_{i,l,k,n}$ is the gas consumption for gas component n from GPP l in bus i in time step k; $q^{ptg}_{i,l,k,n}$ are the gas production of gas component n of PTG l at bus i in time step k; $q_{ij,1,k,n}$ is the gas flow of gas component n in the 1st segment of pipeline ij in time step k; $\chi_{ij,1,k,n}$ and $\chi_{ij,M,k,n}$ are the gas composition of gas component n at the 1st and M_{th} segments in pipeline ij at time step k, respectively; $\chi_{i,k,n}$ is the gas composition of gas component n at bus i in time step k.

3) Terminal condition requirements for linepack energies: Because the gas system is dynamic and operates continuously, it is important to guarantee the terminal state of the gas system should not deviate too much from the initial states. Otherwise, the gas system will be vulnerable and cannot maintain its flexibility to withstand future risks. In the traditional gas system with constant gas composition, the volume of the linepack is usually used as the terminal condition of the gas system control problems [30]. However, when the gas composition is varying, the energy contained in the same volume of gas may be different. Therefore, there we extend the linepack volume into linepack energy, which should be

maintained over a certain level at the end of the MPOEF:

$$\zeta_{ij,k} = A_{ij}/\rho_0 \sum_{m\in\mathcal{M}} \sum_{n\in\mathcal{N}} GCV_n \rho_{ij,m,k} \chi_{ij,m,k,n} \Delta x_{ij} \quad (21)$$

$$\zeta_{ij,K} \geq (1-\beta^{lp})\zeta_{ij,0} \quad (22)$$

where $\zeta_{ij,k}$ is the linepack energy of pipeline ij at time step k; β^{lp} is the threshold coefficient, which is set to maintain the level of linepack energy; K is the total number of the time step.

In addition, it is also important to guarantee the hydrogen has been well accommodated when the MPOEF is over, rather than being stacked somewhere in the gas network. Therefore, we have:

$$(1-\beta^{gc})\chi_{ij,m,0} \leq \chi_{ij,m,K} \leq (1+\beta^{gc})\chi_{ij,m,0} \quad (23)$$

where β^{gc} is the threshold coefficient to guarantee the accommodation of hydrogen.

4) Models of the gas demand and gas source: Considering the gas demand is essentially the gas consumed by gas appliances (e.g., gas water heaters) for combustion, the heat energy of the gas demand should be equal under varying gas compositions. Moreover, the gas composition of the gas demand should be the same as the gas composition in the exact bus. Therefore, we have:

$$GCV^{ng} q^{d,ng}_{i,k} = \sum_{n\in\mathcal{N}} q^{d}_{i,k,n} GCV_n,\ q^{d}_{i,k,n} \geq 0 \quad (24)$$

$$q^{d}_{i,k,n} = \chi_{i,k,n} \sum_{n\in\mathcal{N}} q^{d}_{i,k,n} \quad (25)$$

where GCV^{ng} is the GCV of the original natural gas (without being blended with other gases); $q^{d,ng}_{i,k}$ is the original gas demand measured by natural gas in time step k.

The gas compositions of different gas sources may also vary. Therefore, the gas supply of different gas components in gas sources can be calculated as:

$$q^{s}_{i,l,k,n} = \chi^{s}_{i,l,n} q^{s}_{i,l,k},\ \sum_{n\in\mathcal{N}} x^{s}_{i,l,k,n} = 1, \quad (26)$$

$$q^{s,min}_{i,l} \leq q^{s}_{i,l,k} \leq q^{s,max}_{i,l} \quad (27)$$

where $\chi^{s}_{i,l,n}$ is the molar fraction of the gas component n of gas source l at bus i; $q^{s,max}_{i,l}$ and $q^{s,min}_{i,l}$ are the upper and lower bounds of the gas supply for gas source l at bus i, respectively.

5) Model of gas mixing process: For a specific gas bus, the gas comes from the upper stream components (i.e., upstream pipelines, natural gas sources, PTGs). These gases may have different gas compositions. They will be fully mixed at this gas bus, and then be transported to downstream components (i.e., downstream pipelines, gas loads, GPPs). To model the gas mixing process, we denote the sum of gas component n that flows into the gas bus i at time step k as $q^{in}_{i,k,n}$, and denote the sum of all gas components that flows into the gas bus i at time step k as $q^{in}_{i,k}$. They are mathematically expressed as:

$$q^{in}_{i,k,n} = \sum_{j\in\mathcal{J}_i} \frac{(\gamma_{ij}-1)}{2} q_{ij,1,k,n} + \sum_{l\in\mathcal{L}^{s}_{i}} q^{s}_{i,l,k,n} + \sum_{l\in\mathcal{L}^{ptg}_{i}} q^{ptg}_{i,l,k,n} \quad (28)$$

$$q^{in}_{i,k} = \sum_{n\in\mathcal{N}} q^{in}_{i,k,n} \quad (29)$$

Then, the gas composition at bus i can be calculated by:

$$\chi_{i,k,n} = q^{in}_{i,k,n}/q^{in}_{i,k}, \quad (30)$$

6) Other trivial constraints: Besides the above constraints, there are other trivial constraints required for the gas system to solve the MPOEF problem:

$$q_{ij,m,k} = \sum_{n\in\mathcal{N}} q_{ij,m,k,n} \quad (31)$$

$$|q_{ij,m,k}| \leq q^{max}_{ij} \quad (32)$$

$$p^{min}_{ij} \leq p_{ij,m,k} \leq p^{max}_{ij} \quad (33)$$

$$\chi_{ij,m,k} \sum_{n\in\mathcal{N}} q_{ij,m,k,n} = q_{ij,m,k,n} \quad (34)$$

where q^{max}_{ij} is the capacity of pipeline ij; p^{max}_{ij} and p^{min}_{ij} are the upper and lower bounds of the gas pressure in pipeline ij, respectively.

B. Model of Coupling Components

1) PTG facility: PTG facilities consume surplus renewable generations to produce methane and hydrogen. The relationship between electricity consumption and gas production can be represented by:

$$g^{ptg}_{i,l,k}\eta^{e}_{i,l} = q^{me}_{i,l,k} GCV^{me}/\eta^{me}_{i,l} + q^{hy}_{i,l,k} GCV^{hy} \quad (35)$$

$$q^{hy}_{i,l} \geq 0, q^{me}_{i,l} \geq 0 \quad (36)$$

$$0 \leq g^{ptg}_{i,l,k} \leq g^{ptg,max}_{i,l} \quad (37)$$

where $g^{ptg}_{i,l,k}$ is the electricity consumed by PTG l at bus i in time step k; $\eta^{e}_{i,l}$ and $\eta^{me}_{i,l}$ are the efficiencies of electrolysis and methanation processes, respectively; GCV^{hy} and GCV^{me} are the GCVs of methane and hydrogen, respectively; $q^{hy}_{i,l,k}$ and $q^{me}_{i,l,k}$ are the hydrogen and methane productions of PTG l at bus i in time step k, respectively; $g^{ptg,max}_{i,l}$ is the maximum electricity consumption of the PTG l at bus i.

2) GPP: GPP consumes the gas mixture from the gas system to generate electricity. Similar to the gas demand, the gas composition of the consumed gas by GPP should also be equal to the gas composition at the exact gas bus. Thus, we have:

$$g^{gpp}_{i,l,k} = \eta^{gpp}_{i,l} \sum_{n\in\mathcal{N}} q^{gpp}_{i,l,k,n} GCV_n,\ q^{gpp}_{i,l,k,n} \geq 0 \quad (38)$$

$$q^{gpp}_{i,l,k,n} / \sum_{n\in\mathcal{N}} q^{gpp}_{i,l,k,n} = \chi_{i,k,n} \quad (39)$$

where $g^{gpp}_{i,l,k}$ is the electricity generation of GPP l at bus i in time step k; $\eta^{gpp}_{i,l}$ is the efficiency of the GPP l; $q^{gpp}_{i,l,k,n}$ is the gas component n consumed by the GPP l at bus i in time step k.

C. Model of the Electricity System

The model of the electricity system can be described as:

$$\sum_{l\in\mathcal{L}^{tpp}_{i}} g^{tpp}_{i,l,k} + \sum_{l\in\mathcal{L}^{gpp}_{i}} g^{gpp}_{i,l,k} + \sum_{l\in\mathcal{L}^{rng}_{i}} g^{rng}_{i,l,k} - \sum_{l\in\mathcal{L}^{ptg}_{i}} g^{ptg}_{i,l,k}$$

$$-g^d_{i,k} - \sum_{j\in\mathcal{J}_i} g_{ij,k} = 0 \tag{40}$$

$$g_{ij,k} = (\theta_{i,k} - \theta_{j,k})/X_{ij} \tag{41}$$

$$|g_{ij,k}| \le g^{max}_{ij} \tag{42}$$

$$g^{tpp,min}_{i,l} \le g^{tpp}_{i,l,k} \le g^{tpp,max}_{i,l} \tag{43}$$

$$g^{gpp,min}_{i,l} \le g^{gpp}_{i,l,k} \le g^{gpp,max}_{i,l} \tag{44}$$

$$g^{rng,min}_{i,l} \le g^{rng}_{i,l,k} \le g^{rng,max}_{i,l} \tag{45}$$

where $\mathcal{L}^{rng}_i$ is the set of renewable generators at bus i; $g^{rng}_{i,l,k}$ is the electricity generations of renewable generator l at bus i in time step k; $g^d_{i,k}$ is the electricity demand at bus i in time step k; $g_{ij,k}$ is the electricity flow on branch ij in time step k; $\theta_{i,k}$ is the phase angle of the voltage at bus i in time step k; X_{ij} is the reactance of branch ij; g^{max}_{ij} is the capacity of the electricity branch ij; $g^{tpp,max}_{i,l}$, $g^{tpp,min}_{i,l}$, $g^{gpp,max}_{i,l}$, $g^{gpp,min}_{i,l}$, $g^{rng,max}_{i,l}$, and $g^{rng,min}_{i,l}$ are the upper and lower bounds of TPPs, GPPs, and renewable generators, respectively.

IV. Solution Method

A. SOC Reformulation of MPOEF Problem

The nonlinearity of the MPOEF problem mainly comes from the following three sets of constraints: 1) the discretized form of the PDEs, such as the quadratic-over-linear terms in (12) and (13). 2) the bilinear terms in the gas state equation (14), gas composition limits for gas demands (25) and GPPs (39), as well as the gas mixing equations (30). Although the SOC relaxation technique has been introduced to convexify the gas flow equations with constant compositions [31], this technique can not be applied to our nonlinear constraints due to the variability of $r_{ij,m,k}$. Hence, here we develop the SOC relaxation in a new form by introducing an auxiliary variable $\psi^{mo}_{ij,m,k}$:

$$\left|\left| \begin{matrix} \Delta x^{-\frac{1}{2}}(\overline{\rho}_{ij,m,k} + \Delta p^x_{ij,m,k}), \\ (\frac{\rho_0}{A_{ij}\Delta t})^{\frac{1}{2}}(\overline{\rho}_{ij,m,k} + \Delta q^t_{ij,m,k}), \\ 2\Theta_{ij}\overline{q}_{ij,m,k} \end{matrix} \right|\right| \le \psi^{mo}_{ij,m,k} \tag{46}$$

$$\left|\left| \begin{matrix} \Delta x^{-\frac{1}{2}}(\overline{\rho}_{ij,m,k} - \Delta p^x_{ij,m,k}), \\ (\frac{\rho_0}{A_{ij}\Delta t})^{\frac{1}{2}}(\overline{\rho}_{ij,m,k} - \Delta q^t_{ij,m,k}) \end{matrix} \right|\right| \le \psi^{mo}_{ij,m,k} \tag{47}$$

Above is the pair of SOC constraints for motion equations when $\gamma_{ij} = 1$. If $\gamma_{ij} = -1$, similar SOC constraints can also be derived.

The advective transport equation can be relaxed similarly. Set an auxiliary variable $\psi^{at}_{ij,m,k,n}$, $(\psi^{at}_{ij,m,k,n})^2 = A_{ij}\Delta x(\overline{\rho}_{ij,m,k} + \chi^t_{ij,m,k,n})^2 + \Delta t\rho_0(\overline{q}_{ij,m,k} + \Delta\chi^x_{ij,m,k,n})^2$. Then, we can have a pair of SOC constraints:

$$\left|\left| \begin{matrix} (\rho_0\Delta t)^{-\frac{1}{2}}(\Delta\chi^t_{ij,m,k,n} + \overline{\rho}_{ij,m,k}), \\ (A_{ij}\Delta x)^{-\frac{1}{2}}(\Delta\chi^x_{ij,m,k,n} + \overline{q}_{ij,m,k,n}) \end{matrix} \right|\right| \le \psi^{at}_{ij,m,k} \tag{48}$$

$$\left|\left| \begin{matrix} (\rho_0\Delta t)^{-\frac{1}{2}}(\Delta\chi^t_{ij,m,k,n} - \overline{\rho}_{ij,m,k}), \\ (A_{ij}\Delta x)^{-\frac{1}{2}}(\Delta\chi^x_{ij,m,k,n} - \overline{q}_{ij,m,k}) \end{matrix} \right|\right| \le \psi^{at}_{ij,m,k,n} \tag{49}$$

To drive the relaxation tight, two methods, namely, the penalty term method and the sequential SOC programming are developed. The penalty term method is to drive the SOC relaxation tight preliminarily by adding penalty terms to the objective function. In our case, the penalty term is selected as $\lambda^{mo}\sum_{(ij)\in\mathcal{P}}\sum_{m\in\mathcal{M}}\sum_{k\in\mathcal{K}}(\psi^{mo}_{ij,m,k})^2 + \lambda^{at}\sum_{(ij)\in\mathcal{P}}\sum_{m\in\mathcal{M}}\sum_{k\in\mathcal{K}}\sum_{n\in\mathcal{N}}(\psi^{at}_{ij,m,k,n})^2$, where λ^{mo} and λ^{at} are the penalty coefficients for motion and advective transport equations, respectively.

In sequential SOC programming, the other side of the SOC inequality is approximated by the 1st-order Taylor series:

$$\begin{aligned}(\psi^{mo}_{ij,m,k})^2 \le{}& \Delta x^{-1}\Big((\overline{\rho}^*_{ij,m,k} + \Delta p^{x*}_{ij,m,k})^2 + 2(\overline{\rho}^*_{ij,m,k} \\ &+\Delta p^{x*}_{ij,m,k})(\overline{\rho}_{ij,m,k} - \overline{\rho}^*_{ij,m,k} + \Delta p^x_{ij,m,k} - \Delta p^{x*}_{ij,m,k})\Big) \\ &+(\frac{\rho_0}{A_{ij}\Delta t})^{-1}\Big((\overline{\rho}^*_{ij,m,k} + \Delta q^{t*}_{ij,m,k})^2 + 2(\overline{\rho}^*_{ij,m,k} + \Delta q^{t*}_{ij,m,k}) \\ &(\overline{\rho}_{ij,m,k} - \overline{\rho}^*_{ij,m,k} + \Delta q^t_{ij,m,k} - \Delta q^{t,*}_{ij,m,k})\Big) + 4\Theta^2_{ij} \\ &\Big((\overline{q}^*_{ij,m,k})^2 + 2\overline{q}^*_{ij,m,k}(\overline{q}_{ij,m,k} - \overline{q}^*_{ij,m,k})\Big) + \delta^{mo}_{ij,m,k}\end{aligned} \tag{50}$$

$$\begin{aligned}(\psi^{mo}_{ij,m,k,n})^2 \le{}& A_{ij}\Delta x\Big((\Delta\chi^{t*}_{ij,m,k,n} + \overline{\rho}^*_{ij,m,k})^2 + 2(\chi^{t*}_{ij,m,k,n} \\ &+\overline{\rho}^*_{ij,m,k})(\chi^t_{ij,m,k,n} - \chi^{t*}_{ij,m,k,n} + \overline{\rho}_{ij,m,k} - \overline{\rho}^*_{ij,m,k})\Big) \\ &+\Delta t\rho_0\Big((\Delta\chi^{x*}_{ij,m,k,n} + \overline{q}^*_{ij,m,k})^2 + 2(\chi^{x*}_{ij,m,k,n} + \overline{q}^*_{ij,m,k}) \\ &(\chi^x_{ij,m,k,n} - \chi^{x*}_{ij,m,k,n} + \overline{q}_{ij,m,k} - \overline{q}^*_{ij,m,k})\Big) + \delta^{at}_{ij,m,k,n}\end{aligned} \tag{51}$$

$$\delta^{mo}_{ij,m,k},\ \delta^{at}_{ij,m,k,n} \ge 0 \tag{52}$$

where (50) is the Taylor approximation of another side inequality of (46) when $\gamma_{ij} = 1$. The approximation of another side inequality of (47) when $\gamma_{ij} = 1$, and the approximations of another side inequalities of (46) and (47) when $\gamma_{ij} = -1$ can be derived similarly. Eq. (51) is the Taylor approximation of another side inequality of (48). The approximation of another side inequality of (49) can also be derived similarly. Symbol $(\cdot)^*$ represents the reference value for the corresponding variable, which will be determined in each iteration in the sequential programming, as introduced in the next subsection; $\delta^{mo}_{ij,m,k}$ and $\delta^{at}_{ij,m,k}$ are the slack variables for the Taylor reminders of motion and the advective transport equations, respectively.

The bilinear terms in the gas state equation (14) can be approximated as:

$$\begin{aligned}p_{ij,m,k} = z_{ij,m,k}T_0\Big(&r^*_{ij,m,k}\rho^*_{ij,m,k} + r^*_{ij,m,k}(\rho_{ij,m,k} \\ &-\rho^*_{ij,m,k}) + (r_{ij,m,k} - r^*_{ij,m,k})\rho^*_{ij,m,k}\Big) + \delta^{es}_{ij,m,k}\end{aligned} \tag{53}$$

where $\delta^{es}_{ij,m,k}$ is the Taylor reminder of (53). It can also be incorporated into the framework of sequential programming. Other bilinear constraints can be handled similarly.

B. Sequential SOC Programming Procedures

The basic idea of sequential programming is that, by controlling the slack variables, the optimization problem can be tentatively solved with certain violations of constraints first, and then converged to the optimum as iteration proceeds. The specific procedures are elaborated as follows:

Step 1: Initialize IEGS parameters and wind speed data. Initialize the length step and time step for PDEs. Initialize the penalty $\alpha^{mo,(0)}$, $\alpha^{at,(0)}$, $\alpha^{at,(0)}$, $\alpha^{es,(0)}$, and $\alpha^{re,(0)}$, as well as their upper bounds $\alpha^{mo,max}$, $\alpha^{at,max}$, $\alpha^{es,max}$, $\alpha^{re,max}$. Set the residual tolerance for the sequential programming ϵ.

Step 2: For each time step k, given the wind speed, solve the steady-state-based optimal energy flow problem with alternative gas injections according to [16]. Set the solutions at $k=1$ as the initial condition for PDEs (e.g., $\hat{p}_{ij,m}$, $\hat{q}_{ij,m}$, etc.). Set the solutions at each time step k as the initial reference values for the sequential programming (e.g.,$p^*_{ij,m,k}$, $q^*_{ij,m,k}$, etc.). Set the iteration index for sequential programming $v=1$.

Step 3: In the v_{th} iteration, solve the following SOC programming problem by the given reference points:

$$\begin{aligned}\min \quad f^{(v)} = C^T + \sum_{k\in\mathcal{K}} \Bigg(\sum_{(ij)\in\mathcal{GP}} \sum_{m\in\mathcal{M}} \Bigg(& \lambda^{mo}(\psi^{mo}_{ij,m,k})^2 \\ & + \alpha^{mo,(v)}\delta^{mo,(v)}_{ij,m,k} + \alpha^{se,(v)}\delta^{se,(v)}_{ij,m,k} \\ & + \sum_{n\in\mathcal{N}} (\lambda^{at}(\psi^{at}_{ij,m,k,n})^2 + \alpha^{at,(v)}\delta^{at,(v)}_{ij,m,k,n}) \Bigg) \\ & + \sum_{i\in\mathcal{I}} \sum_{n\in\mathcal{N}} \alpha^{re,(v)}\delta^{re,(v)}_{i,m,n,k} \Bigg) \end{aligned} \tag{54}$$

subject to: (14)-(53) and $\boldsymbol{\chi}_{i,k} \in \mathbb{H}$ (as defined in Section II). By solving the problem above, the solution in v_{th} iteration can be obtained.

Step 4: Check if all the state variables of the IEGS do not change compared with the last iteration, and if all the Taylor reminders converge to zero. For example:

$$|f^{(v)} - f^{(v-1)}|/(f^{(v)} + f^{(v-1)}) \le \epsilon \tag{55}$$

$$\sum_{k\in\mathcal{K}} \Bigg(\sum_{(ij)\in\mathcal{GP}} \sum_{m\in\mathcal{M}} \Bigg(\delta^{mo,(v)}_{ij,m,k} + \sum_{n\in\mathcal{N}} \delta^{at,(v)}_{ij,m,k,n} + \alpha^{se,(v)}\delta^{se,(v)}_{ij,m,k} \Bigg) + \sum_{i\in\mathcal{I}} \sum_{n\in\mathcal{N}} \delta^{re,(v)}_{i,m,n,k} \Bigg) \le \epsilon \tag{56}$$

If yes, end the sequential programming and output the solution as the final result. If no, set the solution in v_{th} iteration as the reference value. Update the penalty coefficients as follows (other penalty coefficients can be updated similarly), and repeat from **Step 3**.

$$\alpha^{mo,(v+1)} = \min\left\{\kappa\alpha^{mo,(v)}, \alpha^{mo,max}\right\} \tag{57}$$

where κ is the multiplier for the penalty coefficients.

V. Case Studies

In this section, an IEGS test case is used to validate the proposed MPOEF model and solution method. It consists of an IEEE 24 bus RTS [32] and Belgium gas transmission system [33]. Following modifications are made: 1) the two energy systems are topologically coupled according to Fig. 3; 2) the generator # 1, 2, 5, 6, 9-11, and 16-20 are replaced with GPPs (the index of the generator can be found in [32]); 3) the generator #23 is replaced by an 800 MW wind farm; 4) the hydrogen production capacities of PTGs are set to 2 Mm^3/day. The simulation period is 24 hours. The optimization is performed on a desktop with Intel(R) Core(TM) i7-10700 CPU @2.90GHz and 16 GB RAM.

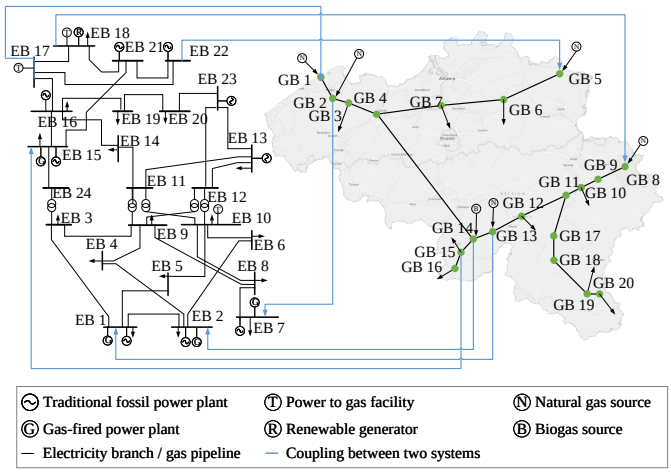

Fig. 3. IEGS test system.

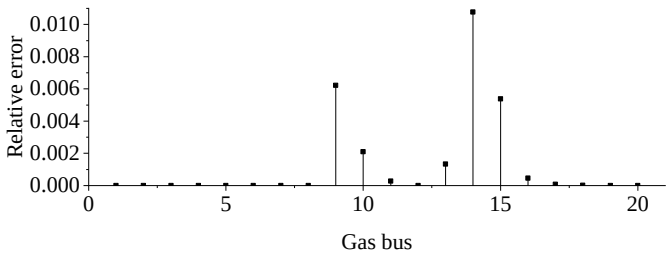

Fig. 4. Relative errors of gas compositions in different gas buses.

A. Validation of Proposed MPOEF

1) Computation performance: In this subsection, the effectiveness of our method is validated. In this case, only the PTG at gas bus #8 is available. The wind generation capacity is zero from the beginning, and changes to 800 MW after one hour. We compare our method with a traditional nonlinear solver (IPOPT), where the optimization problem retains its original nonlinear form. The computation time of our method is 29.82s, which is 97.64% faster than the traditional nonlinear solver. Moreover, by regarding the solutions of the nonlinear solver as the baseline, the relative errors at different gas buses with our method are shown in Fig. 4. As we can see, the errors at all buses are controlled within 1.1%. The maximum relative error appears at gas bus #14 where the gases are mixed.

2) Selections of time and length steps: Four scenarios S1-S4 are compared to determine the appropriate time and length steps for discretizing PDEs. The settings of the four scenarios are marked in Fig. 5. The computation times for these four scenarios are 35.88, 29.82, 22.13, and 12.32s, respectively.

We take S1 as the baseline. As we can see, with the increase of the length step, the relative error increases. The error in S2 is relatively small, and the average value is 5.30×10^{-4}

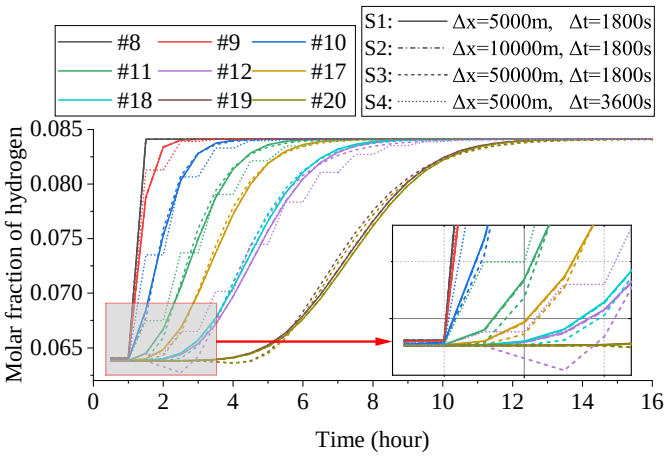

Fig. 5. Comparison with different time and length steps.

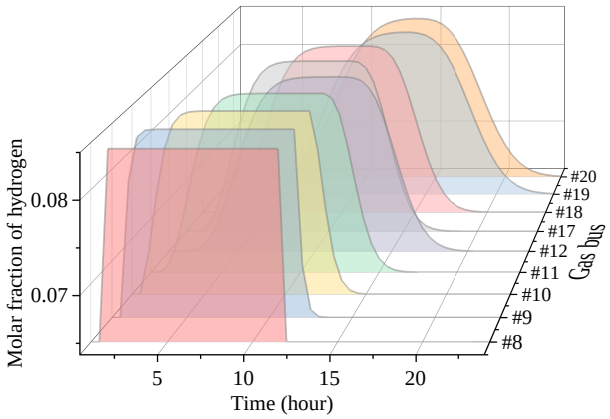

Fig. 6. Operating condition of IEGS: (a) PTG production; (b) traveling of the molar fraction of hydrogen.

during the whole transient process. However, as the length step increases to 50000 m, the mean relative error increases to 0.18 %. We also observed that the maximum error occurs at the beginning, as shown by the purple dash line in S3. The maximum error could be up to 2.58%. In contrast, the dotted line in S2 is always very close to the baseline throughout the transient process. The computation times of these three scenarios are relatively close. Therefore, judging by the accuracy, here we select the size of the length step as 10000 m.

The selection of the time step mainly depends on the required time resolution. We also notice an unneglectable error between S1 and S4, especially just before the molar fraction of hydrogen approaches the steady-state value. Thus, in the following case studies, the time step Δt is selected as 1800s.

B. Traveling of Alternative Gas

This subsection demonstrates the effectiveness of the proposed MPOEF method in tracking the traveling of alternative gas concentrations. It is similar to the last case, except that the wind generating capacity recovers to 0 MW at $t = 12$ h.

The propagation of the hydrogen content along the critical pipeline route, i.e., from gas bus #8-16, is presented in Fig. 6. As we can see, the hydrogen content which is injected into gas bus #8 gradually travels to distant locations along the pipeline route. The molar fraction of hydrogen increases immediately

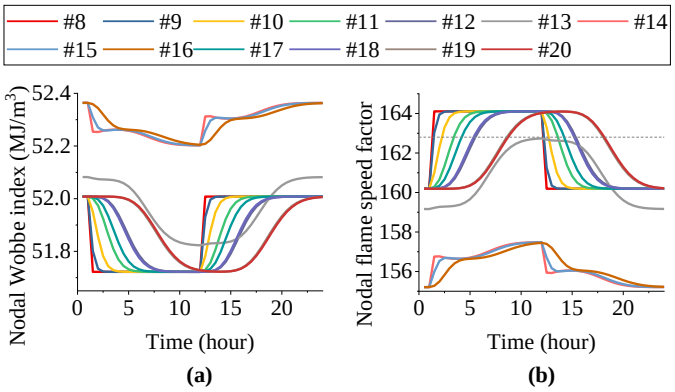

Fig. 7. Security indices: (a) Wobbe index; (b) Weaver flame speed factor.

to 8.43 % after the injection at $t = 1$ h at gas bus #8. In contrast, the molar fraction of hydrogen at gas bus #20 reaches its maximum value at t=13.5 h. The total settling time is 9 h. This indicates that considering the traveling time of hydrogen content in the MPOEF is very necessary. Otherwise, it will lead to miscalculations in the gas composition distribution in the gas network.

Several security indices, i.e., the Wobbe index and flame speed factor, at the representative gas buses are further presented in Fig. 7. As we can see, these security indices are tightly dependent on the molar fraction of hydrogen. For example, for gas buses #8-12 and 17-20, when they reach the peak value of hydrogen fraction, the Wobbe indices become lowest (52.00 MJ/m^3). Although it is lower than the Wobbe index of original natural gas, it does not violate the lower limit (50.22 MJ/m^3). In contrast, the propagation of hydrogen content significantly impacts the flame speed factor. Many buses, including #8-12 and 17-20, violate the upper bound temporarily after the hydrogen travels to their locations. This indicates that during operation, it is necessary to track the real-time traveling of hydrogen concentrations to ensure the security of each gas bus.

C. Multi-Period Operation Results

After validating the effectiveness of the proposed MPOEF method, we applied it to the multi-period operation in this section. All the PTGs are available in this section. The wind data are acquired from [34]. Three scenarios S1-S3 are compared. In S1, the security constraints are not considered. In S2 and S3, the security indices are limited to ±10% and ±5% of their values of original natural gas, respectively.

First, the gas production of PTGs is compared in Fig. 8. We can find that generally in all the scenarios, the gas production of PTGs coincides with the trend of wind speed. For example, during 10:30-17:30, PTG #3 reaches its maximum gas production capacity due to the higher wind speed. Comparing different scenarios, we find that as the security limits become tighter, the hydrogen production of PTGs decreases. Instead, they choose to convert more hydrogen into methane, because methane has closer interchangeability compared to natural gas. For example, the total methane production in S1 is zero, while it increases to 9.85% of the total gas production in S2. This number further increases to 27.72% in S3.

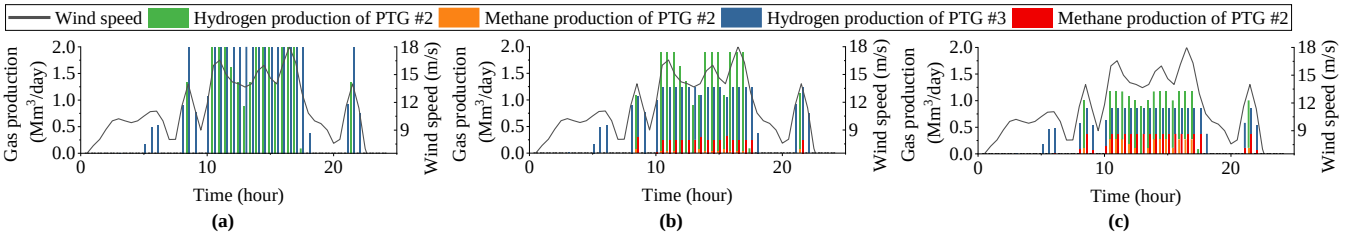

Fig. 8. Gas productions of PTGs: (a) S1; (b) S2; (c) S3.

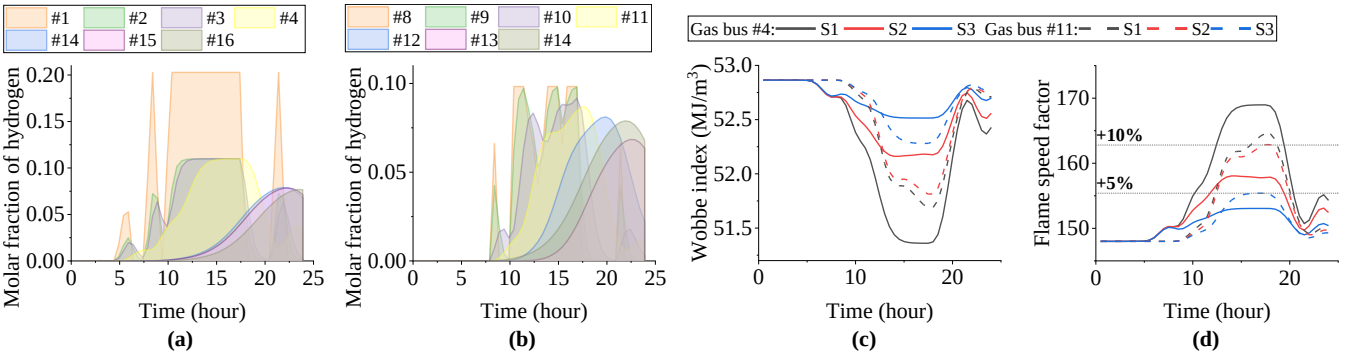

Fig. 9. Gas composition and security indices: (a) molar fractions of hydrogen from gas buses#1-4-16; (b) molar fractions of hydrogen from gas buses #8-14; (c) Wobbe indices at gas buses #4 and 11; (d) flame speed factors at gas buses #4 and 11.

The traveling of hydrogen in different critical pipeline routes, as well as the mixing process in S1, are demonstrated in Fig. 9 (a)-(b). We find that the molar fractions of hydrogen at injection points are in line with the hydrogen productions of PTGs. For example, the molar fraction of hydrogen at gas bus #1 increases from zero to around 20% immediately at 8:30, just when the hydrogen production of PTG #3 begins to increase. Then, as the hydrogen travels in the gas network, its molar fraction will be diluted both by injection of natural gas by gas sources (e.g., the gas source at gas bus #2), or by the advection in the pipeline (e.g. gas bus #3-4). It can also be diluted by gas mixing processes. For example, the peak value of hydrogen molar fraction at gas bus #4 is 10.98% at 17:30, which takes approximately 4.5 h to travel to gas bus #14. At 22:00, it is diluted by the gas mixture from #13 (with 6.74% hydrogen). Then, the hydrogen molar fraction of the mixture at gas bus #14 is reduced to 7.82%.

The security indices in three scenarios are compared in Fig. 9(c)-(d). We find that with the injection of hydrogen, the Wobbe index tends to decrease, while the flame speed factor tends to increase. For example, the Wobbe index at gas bus #4 in S1 is 2.25% lower than that in S3. We also find that the flame speed factor is more critical than the Wobbe index for the regulation of hydrogen injection. Even in S1, the Wobbe index does not violate the lower limit. On the contrary, in S2 and S3, the flame speed factor at gas bus #11 reaches their upper bounds, respectively. It validates that our MPOEF successfully contains the security indices within the acceptable range, while the accommodation of green hydrogen can also be maximized. It also validates the necessity of adding the flame speed factor as an additional index to the traditional Dutton method, which can keep the security of a hydrogen-blended gas system.

The variations of linepack energies in these scenarios are demonstrated in Fig. 10. We can see that although the linepack

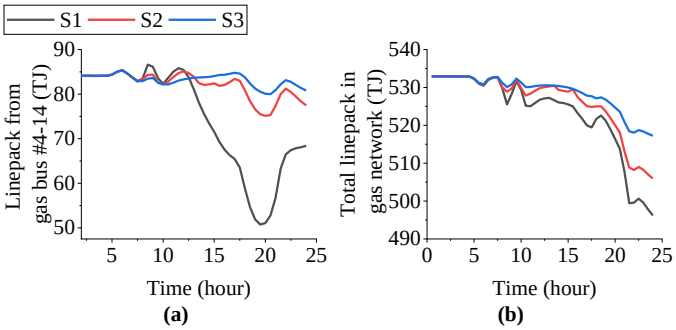

Fig. 10. (a) Linepack energies in the pipeline connecting gas buses #4 and 14; (b) total linepack energies in the gas network.

energy varies with the wind power and hydrogen injection, they are still maintained within the acceptable range. For example, in the pipeline that connects gas buses #4-14, as shown in Fig. 10 (a), the linepack energy decrease dramatically at 20:00 with the large volume of hydrogen injection. However, it recovers to the normal level at the end of the operation. We also find that with tighter security limits, the variation in the linepack is also minor. For example, as shown in Fig. 10 (b), the total linepack energy in the gas system at 24:00 in S3 is 4.07% higher than that in S1. Since the linepack energy plays an important role in maintaining the flexibility of the gas system, the hydrogen injection can jeopardize that flexibility in some sense. Therefore, apart from the security indices, we should also pay close attention to linepack energies when injecting hydrogen into the gas system.

VI. Conclusions

This paper proposes an MPOEF model and a tractable solution method for IEGS with alternative gas. The dynamics of gas composition are characterized to reveal the traveling of hydrogen concentrations, as well as its impact on the physical property of the gas network in real-time. Numerical

results show that the proposed solution method is 97.64% faster than general nonlinear solvers, while the relative error is controlled within 1.1%. The result of the MPOEF shows the importance of considering the gas composition dynamics. The hydrogen content takes about 12.5 hours to travel from the injection point to the end of the pipeline route. Inaccuracies will be caused if we neglect this considerable traveling time. Moreover, we find that the flame speed factor is a more critical factor than other security indices. With different security limits, the accommodation of renewable energies, the gas production mode of PTGs, and the linepack energies will be different. A looser security limit will lead to a lower linepack energy, which may affect the flexibility of the gas system.

With the growing attention to the use of alternative gas in decarbonized energy systems, the proposed MPOEF technique can provide a powerful tool for system operators to regulate the safety of IEGS during operation. It can also be extended to help with the short-term reliability evaluation or unit commitment issues with ensured gas safety in hydrogen-blended energy systems in the near future.

REFERENCES

[1] Z. Zhang, C. Wang, H. Lv, F. Liu, H. Sheng, and M. Yang, "Day-ahead optimal dispatch for integrated energy system considering power-to-gas and dynamic pipeline networks," *IEEE Transactions on Industry Applications*, vol. 57, no. 4, pp. 3317–3328, Apr. 2021.

[2] HyDeploy Project – Project Close Down Report. [Online]. Available: https://hydeploy.co.uk/app/uploads/2022/06/HyDeploy-Close-Down-Report_Final.pdf.

[3] Launch of Hebei's first demonstration project on natural gas with hydrogen blending. [Online]. Available: https://news.bjx.com.cn/html/20200917/1105156.shtml.

[4] T. Briggs, "The combustion and interchangeability of natural gas on domestic burners," *Combustion*, vol. 4, no. 3, 2014.

[5] D. Haeseldonckx and W. D'haeseleer, "The use of the natural-gas pipeline infrastructure for hydrogen transport in a changing market structure," *International Journal of Hydrogen Energy*, vol. 32, no. 10-11, pp. 1381–1386, Jul-Aug. 2007.

[6] M. Abeysekera, J. Wu, N. Jenkins, and M. Rees, "Steady state analysis of gas networks with distributed injection of alternative gas," *Applied Energy*, vol. 164, pp. 991–1002, Feb. 2016.

[7] S. Pellegrino, A. Lanzini, and P. Leone, "Greening the gas network – the need for modelling the distributed injection of alternative fuels," *Renewable and Sustainable Energy Reviews*, vol. 70, pp. 266–286, Apr. 2017.

[8] M. Cavana, A. Mazza, G. Chicco, and P. Leone, "Electrical and gas networks coupling through hydrogen blending under increasing distributed photovoltaic generation," *Applied Energy*, vol. 290, p. 116764, May. 2021.

[9] L. Cheli, G. Guzzo, D. Adolfo, and C. Carcasci, "Steady-state analysis of a natural gas distribution network with hydrogen injection to absorb excess renewable electricity," *International Journal of Hydrogen Energy*, vol. 46, no. 50, pp. 25 562–25 577, Jul. 2021.

[10] S. Zhang, S. Wang, Z. Zhang, J. Lyu, H. Cheng, M. Huang, and Q. Zhang, "Probabilistic multi-energy flow calculation of electricity–gas integrated energy systems with hydrogen injection," *IEEE Transactions on Industry Applications*, Mar-Apr. 2022.

[11] D. Zhou, S. Yan, D. Huang, T. Shao, W. Xiao, J. Hao, C. Wang, and T. Yu, "Modeling and simulation of the hydrogen blended gas-electricity integrated energy system and influence analysis of hydrogen blending modes," *Energy*, vol. 239, p. 121629, Jan. 2022.

[12] I. Saedi, S. Mhanna, and P. Mancarella, "Integrated electricity and gas system modelling with hydrogen injections and gas composition tracking," *Applied Energy*, vol. 303, p. 117598, Dec. 2021.

[13] A. De Corato, I. Saedi, S. Riaz, and P. Mancarella, "Aggregated flexibility from multiple power-to-gas units in integrated electricity-gas-hydrogen distribution systems," *Electric Power Systems Research*, vol. 212, p. 108409, Nov. 2022.

[14] P. Zhao, C. Gu, Z. Hu, D. Xie, I. Hernando-Gil, and Y. Shen, "Distributionally robust hydrogen optimization with ensured security and multi-energy couplings," *IEEE Transactions on Power Systems*, vol. 36, no. 1, pp. 504–513, Jun. 2020.

[15] P. Zhao, X. Lu, Z. Cao, C. Gu, Q. Ai, H. Liu, Y. Bian, and S. Li, "Volt-var-pressure optimization of integrated energy systems with hydrogen injection," *IEEE Transactions on Power Systems*, vol. 36, no. 3, pp. 2403–2415, Oct. 2021.

[16] S. Wang, J. Zhai, and H. Hui, "Optimal energy flow in integrated electricity and gas systems with injection of alternative gas," *IEEE Transactions on Sustainable Energy*, (Early access). 2023.

[17] J. Yang, N. Zhang, C. Kang, and Q. Xia, "Effect of natural gas flow dynamics in robust generation scheduling under wind uncertainty," *IEEE Transactions on Power Systems*, vol. 33, no. 2, pp. 2087–2097, Jul. 2017.

[18] S. Wang, Y. Ding, X. Han, P. Wang, L. Goel, and J. Ma, "Short-term reliability evaluation of integrated electricity and gas systems considering dynamics of gas flow," *IET Generation, Transmission & Distribution*, vol. 15, no. 20, pp. 2857–2871, 2021.

[19] D. Zhou, C. Wang, S. Yan, Y. Yan, Y. Guo, T. Shao, T. Li, X. Jia, and J. Hao, "Dynamic modeling and characteristic analysis of natural gas network with hydrogen injections," *International Journal of Hydrogen Energy*, vol. 47, no. 78, pp. 33 209–33 223, Sep. 2022.

[20] Z. Zhang, I. Saedi, S. Mhanna, K. Wu, and P. Mancarella, "Modelling of gas network transient flows with multiple hydrogen injections and gas composition tracking," *International Journal of Hydrogen Energy*, vol. 47, no. 4, pp. 2220–2233, Dec. 2022.

[21] D. Zhou, X. Jia, Z. Peng, and Y. Ma, "Coordinate control law analysis for hydrogen blended electricity-gas integrated energy system," *International Journal of Hydrogen Energy*, vol. 47, no. 69, pp. 29 648–29 660, Aug. 2022.

[22] S. Mhanna, I. Saedi, P. Mancarella, and Z. Zhang, "Coordinated operation of electricity and gas-hydrogen systems with transient gas flow and hydrogen concentration tracking," *Electric Power Systems Research*, vol. 211, p. 108499, Oct. 2022.

[23] Gas Safety (Management) Regulations. [Online]. Available: https://www.legislation.gov.uk/uksi/1996/551/introduction/made.

[24] C. Park, S. Oh, C. Kim, Y. Choi, and Y. Ha, "Effect of natural gas composition and gas interchangeability on performance and emission characteristics in an air–fuel controlled natural gas engine," *Fuel*, vol. 287, p. 119501, Mar. 2021.

[25] M. Bus, "Review of the impact of hydrogen addition to natural gas on gas turbine combustion," Jun. 2013. [Online]. Available: http://essay.utwente.nl/69334/

[26] C. S. Weaver, "Natural gas vehicles—a review of the state of the art," *SAE transactions*, vol. 98, pp. 1190–1210, 1989.

[27] A. Osiadacz, "Simulation of transient gas flows in networks," *International Journal for Numerical Methods in Fluids*, vol. 4, no. 1, pp. 13–24, 1984.

[28] M. J. Ryan and R. L. Mailloux, "Methods for performing composition tracking for pipeline networks," in *PSIG Annual Meeting*. OnePetro, 1986.

[29] E. S. Menon, *Gas pipeline hydraulics*. Crc Press, 2005.

[30] A. Zlotnik, L. Roald, S. Backhaus, M. Chertkov, and G. Andersson, "Coordinated scheduling for interdependent electric power and natural gas infrastructures," *IEEE Transactions on Power Systems*, vol. 32, no. 1, pp. 600–610, Mar. 2017.

[31] Y. He, M. Yan, M. Shahidehpour, Z. Li, C. Guo, L. Wu, and Y. Ding, "Decentralized optimization of multi-area electricity-natural gas flows based on cone reformulation," *IEEE Transactions on Power Systems*, vol. 33, no. 4, pp. 4531–4542, Dec. 2018.

[32] C. Grigg, P. Wong, P. Albrecht, R. Allan, M. Bhavaraju, R. Billinton, Q. Chen, C. Fong, S. Haddad, S. Kuruganty *et al.*, "The IEEE reliability test system-1996. A report prepared by the reliability test system task force of the application of probability methods subcommittee," *IEEE Transactions on Power Systems*, vol. 14, no. 3, pp. 1010–1020, Aug. 1999.

[33] D. De Wolf and Y. Smeers, "The gas transmission problem solved by an extension of the simplex algorithm," *Management Science*, vol. 46, no. 11, pp. 1454–1465, Nov. 2000.

[34] National oceanic and atmospheric administration. [Online]. Available: https://www.noaa.gov/.